A New Robust Algorithm to Improve the Dynamic Performance on the Speed Control of Induction Motor Drive

Guang Feng, *Student Member, IEEE*, Yan-Fei Liu, *Senior Member, IEEE*, and Lipei Huang

***Abstract*—A nonlinear auto-disturbance rejection controller (ADRC) has been developed to ensure high dynamic performance of induction motors in this paper. By using the extended state observer (ESO), ADRC can accurately estimate the derivative signals and precise decoupling of induction motors is achieved. In addition, the proposed strategy realizes the disturbance compensation without accurate knowledge of induction motor parameters. The simulation and experimental results show that the proposed controller ensures good robustness and adaptability under modeling uncertainty and external disturbance. It is concluded that the proposed topology produces better dynamic performance, such as small overshoot and fast transient time, than the conventional proportional/integral/derivative (PID) controller in its overall operating conditions.**

***Index Terms*—Auto-disturbance rejection controller (ADRC), extended state observer (ESO), robustness.**

I. Introduction

THE FIELD-oriented control (FOC) technique is widely used in high performance motion control of induction motors. Because of torque/flux decoupling, FOC achieved good dynamic response and accurate motion control as dc motors. However, in real-time implementation, precise decoupling which requires accurate motor parameters cannot be completely achieved due to significant plant uncertainties. These uncertainties include external disturbances, unpredictable parameter variations, and unmodeled plant nonlinear dynamics. Consequently, this will deteriorate the dynamic performance of flux and speed significantly. Generally speaking, the performance of this control system depends on the accuracy of the mathematical model of induction motors [1].

This paper introduces a new configuration called auto-disturbance rejection controller (ADRC) into the control of induction motors. The auto-disturbance rejection controller, which is inherently suitable for dealing with the system uncertainties, generates very good static and dynamic performance, even in the presence of a large and fast variation of motor parameters and load disturbances. The core of ADRC is the extended state observer (ESO), which is based on the concept of generalized derivatives and generalized functions. Using the extended state observer, the ADRC can realize accurate decoupling of induction motors. In addition, the impact of external disturbances and parameter variations could also be estimated and compensated by the ADRC. Therefore, the accurate knowledge of the induction motor model is not required. As a result, the design of ADRC is inherently independent of the controlled system model and its parameters. Therefore, this controller has the advantage of good adaptability and robustness. This paper presents a detailed comparison of the ADRC and the conventional proportional/integral/derivative (PID) controller under different operating conditions based on simulation and experimental results. It is shown that the proposed controller can provide not only good speed regulation, but also excellent speed dynamic performance under large variations of drive system parameters and load conditions.

Manuscript received January 20, 2003; revised October 15, 2003. Recommended by Associate Editor M. G. Simoes.

G. Feng and Y.-F. Liu are with the Department of Electrical and Computer Engineering, Queen's University, Kingston, ON K7L 3N6, Canada (e-mail: guang.feng@ece.queensu.ca; yanfei.liu@ece.queensu.ca).

L. Huang is with the Department of Electrical Engineering, Tsinghua University, Beijing 100084, China (e-mail: huanglipei@tsinghua.edu.cn).

Digital Object Identifier 10.1109/TPEL.2004.836619

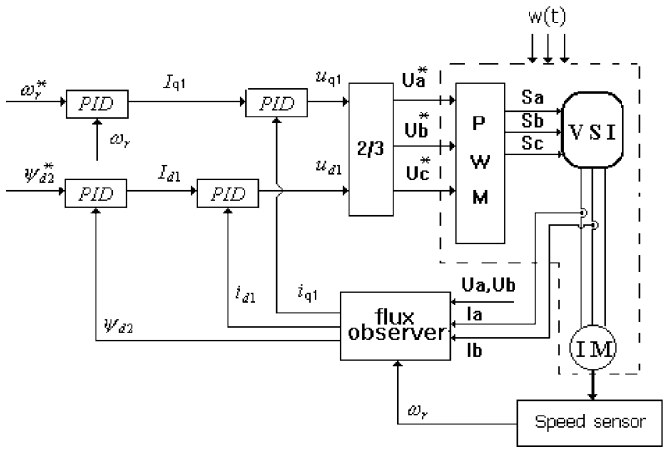

Fig. 1. Control system of induction motor using PID controllers.

II. Control Strategy

A. Limitations of Conventional Vector Control in Speed Regulation of Inductor Motor

In the conventional FOC, PID regulators are used to control the flux magnitude, rotor speed, and currents independently (shown in Fig. 1), where $w(t)$ represents the overall effect of external disturbances, parameter variations, and plant nonlinear dynamics. The part surrounded by dashed line is the system/object under control. In PID controllers, the derivatives of the signals are required in order to achieve control objectives, such as reduced response time and reduced overshoot during transient conditions. Unfortunately, the derivatives of signals are

difficult to retrieve because of noise. Furthermore, due to nonlinearities and uncertainties existing in the induction machine drive system, it is difficult for the conventional PID controller to achieve good static and dynamic performance for different operating situations. As a consequence of these phenomena, a degradation of drive performance occurs.

To avoid these problems, a great deal of research has been done involving alternative control techniques. In recent years, adaptive methods and predictive PID controllers have become more attractive in the improvement of the robustness and dynamic performance of control systems [2]–[6]. However, they are very complex and require knowledge of model parameters and model states. As a consequence, they require high computational intensity in real-time implementation.

One effective way to design a controller is to get rid of the restriction of the mathematical model. This would promote a new structure of controllers. Based on the theory of nonlinear feedback and generalized derivatives, ADRC is introduced in this paper.

B. Advantages of Nonlinear Feedback Compared With Linear Feedback

In many respects, a nonlinear system has some high efficient characteristics compared to a linear system. To give a simple example, consider the system $\dot{x} = w(t) + u(t)$, where $w(t)$ is the disturbance and the control signal $u(t)$ is designed to stabilize the whole system. Using the linear feedback control $u = -kx$, at the steady-state $\dot{x} = 0$, the steady-state error of the closed loop is $e = w(t)/k$ (assuming $k > |w(t)|$). By choosing nonlinear feedback control $u = -k|x|^{\alpha}\,\mathrm{sign}(x), 0 < \alpha < 1$, where $\mathrm{sign}(x)$ is the signum function. The magnitude of steady-state error is reduced to $|e| = |w(t)/k|^{1/\alpha} < |w(t)/k|$. This indicates that a proper nonlinear feedback control can significantly reduce the effect of disturbance compared with linear feedback.

Giving another example, for system $\dot{x} = -cx + u$, where the input signal is $v(t)$ and c is a constant related to the system. A feedback control $u(t) = f(v(t) - x(t))$ is designed, so that the state variable $x(t)$ can converge to the input signal $v(t)$ quickly. Assuming input $v(t) = v$(constant), the linear feedback control law is chosen as $u = k(v(t) - x(t))$ (k is the feedback coefficient). Then, the steady-state error of the system $e_{\mathrm{linear}}(t) = v(t) - x(t)$ is converged to $v \cdot c/(c+k)$. Appendix A gives the detailed derivation.

However, if a nonlinear feedback control is chosen as $u = k|v(t) - x|^{a}\,\mathrm{sign}(v(t) - x)$ $(0 < \alpha < 1)$, the steady-state error $e_{\mathrm{nonlinear}}(t)$ will be smaller than $(cv/k)^{1/\alpha}$, as shown in Appendix A. Appendix A also illustrates that in condition $0 < \alpha < 1$, $c \ll k$, and $cv \ll k$, which is normally the case, the steady-state error of nonlinear feedback $e_{\mathrm{nonlinear}}$ will be much smaller than that of linear feedback using the same feedback coefficient k. For example, if $c = 1$, $v = 1$, and $k = 100$, the steady-state error, by using linear feedback, is $e_{\mathrm{linear}} = 1/101 \approx 1/100$. By using nonlinear feedback, and assuming $\alpha = 1/2$, the steady-state error $e_{\mathrm{nonlinear}} < (1/100)^2 \ll e_{\mathrm{linear}}$.

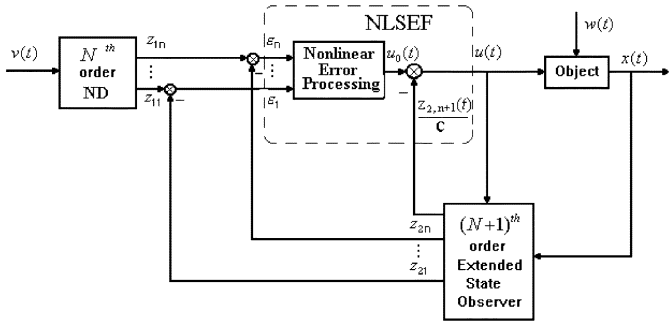

Fig. 2. Block diagram of $Z_i(t)$ order ADRC.

The above examples show that the nonlinear feedback control has the ability to greatly constrain the influence of system modeling and disturbances. They demonstrate that there exists some kind of control strategy, which is independent of the mathematical model of controlled system. Considering one extreme situation, when $\alpha \to 0$, this control system is equivalent to sliding mode control. It has been shown that sliding mode control has robustness and is independent of disturbances and modeling uncertainties. This example indicates that if the nonlinear feedback control is properly designed, it is possible for a nonlinear feedback control system to achieve robustness and adaptability to disturbances and uncertainties.

C. Principle of ADRC

Based on the nonlinear feedback, the nonlinear auto-disturbance rejection controller (ADRC) is introduced to achieve high dynamic performance in the overall operating range. It is composed of three parts (shown in Fig. 2): 1) nonlinear differentiator (ND), 2) extended state observer (ESO), and 3) nonlinear state error feedback control law (NLSEF) [7]. The essential part of ADRC is the extended state observer.

Generally speaking, to control any Nth order nonlinear system, $(N+1)$th order ADRC is needed. For any given input reference signal $v(t)$, the Nth order nonlinear differentiator generates the preconditioned transition process $z_{11}(t)$ and it's first to $N-1$th derivatives $z_{12}(t), \ldots, z_{1n}(t)$ (shown in Fig. 2). Based on the theory of a generalized derivative and nonlinear feedback algorithm, the key part of $(N+1)$th order ADRC is the $(N+1)$th order extended state observer (ESO). As shown in Fig. 2, the state variables of ESO, $z_{2i}(t)$ and $i = 1, \ldots, n$, will successfully converge to the observed state variable $x(t)$ and its derivatives. In addition, the $(N+1)$th state of ESO, $z_{2,n+1}(t)$, reveals the information about the overall influence of external and internal disturbances $w(t)$.

By comparing the difference between the outputs of the nonlinear differentiator $z_{1i}(t)$ and those of extended state observer $z_{2i}(t)$, $i = 1, \ldots, n$ (shown in Fig. 2) nonlinear state error feedback control law $u_0(t)$ is used to drive the state trajectory to the desired reference signal. Furthermore, with the help of modeling uncertainty and disturbance observation $z_{2,n+1}(t)$, online compensation is made by $u(t) = u_0(t) - z_{2,n+1}(t)/c$. Details of each part of ADRC will be discussed in Sections III–V.

1) Structure of Extended State Observer (ESO): Based on the theory of generalized derivative and generalized functions, ESO is a nonlinear configuration for observing the states and

disturbances of the system under control without the knowledge of the exact system parameters. Giving an example, for any arbitrary Nth order nonlinear system

$$x^{(n)} = f(x, \dot{x}, \ldots, x^{(n-1)}, t) + w(t) + c \cdot u(t) \tag{1}$$

where $f(t)$ represents the arbitrary system function, $w(t)$ is an unknown disturbance, $u(t)$ is the control law, $x(t)$ is the measurable state variable, and c is the coefficient of control law. Its state space equation can be written as

$$\begin{cases} \dot{x}_1 = x_2 \\ \vdots \\ \dot{x}_{n-1} = x_n \\ \dot{x}_n = f(x, \dot{x}, \ldots, x^{(n-1)}, t) + w(t) + cu \end{cases} \tag{2}$$

where $x_1 = x, x_2 = \dot{x}, \ldots, x_n = x^{(n-1)}$.

Unlike the full order (Nth order) state observer, ESO utilizes $(N+1)$th order (full order plus 1) state observation to achieve state and disturbance estimation [shown in (3)]. After startup, the output of the ESO $z_{21}, \ldots, z_{2n}$ will converge quickly and accurately to the observed states $x_1, x_2, \ldots, x_n$. The initial values of $z_{21}, \ldots, z_{2n}, z_{2,n+1}$ are all set to be zero

$$\begin{cases} \dot{z}_{21} = z_{22} - g_1(z_{21} - x_1(t)) \\ \vdots \\ \vdots \\ \dot{z}_{2n} = z_{2,n+1} - g_n(z_{21} - x_1(t)) + c \cdot u(t) \\ \dot{z}_{2,n+1} = -g_{n+1}(z_{21} - x_1(t)) \end{cases}$$
$$g_i(z_{21} - x_1(t)) = \beta_i fal\,(z_{21} - x_1(t), \alpha, \delta)$$
$$i = 1, \ldots, n+1$$
$$fal(\varepsilon, \alpha_i, \delta) = \begin{cases} |\varepsilon|^{\alpha} \mathrm{sgn}(\varepsilon), & |\varepsilon| > \delta \\ \frac{\varepsilon}{\delta^{1-\alpha}} & |\varepsilon| \le \delta \end{cases} \tag{3}$$

where $\varepsilon = z_{21} - x_1(t)$, sign$(\varepsilon)$ is the signum function. The exponential $\alpha \in (0,1)$ is usually set to be $\alpha = (m/2^n)$ $(n = 1, 2, \ldots,$ and $m \le 2^n)$. α and the scaling factor β_i determine the convergence speed of ESO. The parameter δ determines the nonlinear region of the ESO.

Nonlinear state feedback in the ESO is used to achieve linearization of nonlinear systems [shown in (3)]. As mentioned previously, the derivative signals are often difficult to obtain because of noises. But in the ESO, lower order derivatives (such as $z_{21}(t), \ldots, z_{2n}(t)$) are obtained by integrating the higher order derivatives $(z_{22}(t), \ldots, z_{2,n+1}(t))$. The differential operation is no longer needed. As a result, the differential signal is noise free. The generalized derivatives of given signals will be accurately achieved.

Furthermore, if we define $x_{n+1}(t) = f(x, \dot{x}, \ldots, x^{(n-1)}, t) + w(t)$, where $f(x, \dot{x}, \ldots, x^{(n-1)}, t)$ represents the system modeling uncertainty and $w(t)$ represents the unknown disturbance, then (2) can be rewritten as

$$\begin{cases} \dot{x}_1(t) = x_2(t) \\ \vdots \\ \dot{x}_n(t) = x_{n+1}(t) + c \cdot u(t) \\ \dot{x}_{n+1}(t) = b(t) \end{cases} \tag{4}$$

where $b(t)$ is the variation rate of system uncertainty and disturbance $x_{n+1}(t)$.

Subtracting (4) from (3), the dynamic error equation is defined as

$$\begin{cases} \delta\dot{x}_1 = \delta x_2 - g_1(\delta x_1) \\ \vdots \\ \delta\dot{x}_n = \delta x_{n+1} - g_n(\delta x_1) \\ \delta\dot{x}_{n+1} = -b(t) - g_{n+1}(\delta x_1) \end{cases} \tag{5}$$

where δx_i is $z_{2i} - x_i$ and i is $1, \ldots, n+1$.

For any boundary $b(t)$, when the nonlinear functions $g_i(z)$ and their related parameters α, β_i, and δ are properly selected to constrain the function of system uncertainties and disturbances, the system (5) is asymptotic stable. Under this condition, the state variables of ESO, $z_{2i}(t), i = 1, \ldots, n$, will quickly converge to the observed state variables $x(t)$ and its derivatives $\dot{x}(t), \ddot{x}(t), \ldots, x^{(n-1)}(t)$. Furthermore, the signal of $(N+1)$th state variable $z_{2,n+1}(t)$ reveals the information about the overall impact of external disturbances and plant uncertainties imposed on the system under control. Based on this information, compensation and elimination of disturbances and model uncertainties can be achieved. If the variation rate $b(t)$ has some boundary, the overall effect of the external and internal disturbances $x_{n+1}(t)$ imposed on the system can be observed by $z_{2,n+1}(t)$ successfully, even though the mathematic expression and accurate parameters of $f(t)$ and $w(t)$ may be still unknown. It will greatly enhance the robustness of the control system against the modeling uncertainties and disturbances.

By using the ESO, the whole nonlinear system is decomposed into n integrators in cascade, so the feedback linearization is realized. Similar to input-output feedback linearization, the ESO can be treated as some kind of dynamic feedback linearization. However, its architecture and performance are not determined by the actual expression of system under control, but only affected by the range of its variation rate. Therefore, this observer has good robustness and adaptability. This is the main advantage of this configuration.

2) Structure of Nonlinear Differentiator (ND): The second part of ADRC is a Nth order nonlinear differentiator. The objective of ND is to define a desirable transition response when the input changes. Its input is the reference signal $v(t)$, the output of ND is the premodulated reference signal $z_{11}(t)$ and its derivative $z_{12}(t), \ldots, z_{1n}(t)$ (as shown in Fig. 2).

The mathematic model of nonlinear differentiator is given as (6), shown at the bottom of the next page, where $v(t)$ is the given input reference signal, $z_{11}(t)$ is the premodulated signal of $v(t)$, $z_{12}(t), \ldots, z_{1n}(t)$ are the modulated first to $(N-1)$th order derivatives of $v(t)$, and sgn(ε) is the signum function. r is the scaling factor of ND. It influences the converge speed of ND. $b_1, \ldots, b_{n-1}$ are the fine tuning factors of ND. α and δ serve the same function as that in ESO.

In the conventional PID controller, it is hard to achieve fast response and reduced overshoot at the same time. This is because the PID controller utilizes the original given signals directly. Any sharp change (step change) in the given signal could

lead to overshoot in the output. In the Nth order nonlinear differentiator, the given input signal $v(t)$ is regulated to a continuous smooth curve $z_{11}(t)$, whose derivatives $z_{12}(t),\ldots,z_{1n}(t)$ are also continuous, smooth, and finite. That means ND can smooth the sharp changes in the input signal, so that the ADRC could still maintain no overshoot during the fast transient process, even though the input signal may change suddenly.

It can be seen from (6), that the mathematical function of the nonlinear differentiator is a nonlinear structure with linear intervals near the original point. The merit of this topology is that it can fully utilize the nonlinear characteristics for large signals. At the same time, the phenomenon of chatting near the origin is avoided. In the linear intervals, the nonlinear differentiator acts as a very good low pass filter. Similar to ESO, lower order derivatives [such as $z_{11}(t),\ldots,z_{1,n-1}(t)$] are also achieved by integrating the higher order derivatives $(z_{12}(t),\ldots,z_{1n}(t))$. The contained noises are all constrained, not enlarged, so that ND can get high quality derivatives as well.

3) Structure of Nonlinear State Error Feedback Control Law (NLSEF): As shown in Fig. 2, the nonlinear differentiator generates the arranged transition process and its derivatives $z_{11},\ldots,z_{1n}$. The outputs of extended state observer $z_{21},\ldots,z_{2n}$ estimate the states of a controlled system. By comparing the difference between the outputs of nonlinear differentiator and those of extended state observer (shown in Fig. 2), the nonlinear state error feedback control law $u_0(t)$ is used to drive the state trajectory to the desired reference signal. Its mathematic expression is given as

$$\begin{aligned} u_0 &= k_1 fal(\varepsilon_1,\alpha,\delta)+\cdots+k_n fal(\varepsilon_n,\alpha,\delta)\\ fal(\varepsilon_i,\alpha,\delta) &= \begin{cases} |\varepsilon_i|^{\alpha}\operatorname{sign}(\varepsilon_i), & |\varepsilon_i|>\delta\\ \frac{\varepsilon_i}{\delta^{1-\alpha}}, & |\varepsilon_i|\le\delta \end{cases}\\ i &= 1,\ldots,n \end{aligned} \tag{7}$$

where $\varepsilon_1=z_{11}-z_{21},\varepsilon_2=z_{12}-z_{22},\ldots,\varepsilon_n=z_{1n}-z_{2n}$. k_i $(i=1,\ldots,n)$ is the scaling factor of NLSEF. α and δ are the variable parameters of NLSEF and they serve the same function as that in ESO and ND.

It can be seen from (7), that the nonlinear feedback structure is adopted. In addition, this configuration is independent of the object model. Furthermore, with the help of modeling uncertainty and disturbance estimation $z_{2,n+1}(t)$, online compensation is made by $u(t)=u_0(t)-z_{2,n+1}(t)/c$ [where c is the coefficient of control law in (1)]. The robustness of the system is guaranteed.

4) Advantages of ADRC: From the previous sections, it can be seen that ADRC has many advantages.

a) The generalized derivatives of given signals can be obtained accurately.
b) With the help of nonlinear differentiator, ADRC could maintain no overshoot during the fast transient process, even though the input signal may change suddenly.
c) By using ESO, the whole nonlinear system is decomposed into n integrators in cascade. Decoupling and dynamic feedback linearization are realized.
d) ADRC utilizes the online estimation and compensation to eliminate the steady-state error between input and output. Therefore, integrators are no longer needed. The desired behaviors of the control system such as tracking, regulation, and stability are guaranteed.
e) With the help of ESO and NLSEF, the system uncertainties and external disturbance could be estimated and compensated instantaneously and accurately. The control system's robustness is guaranteed.
f) The architecture and performance of all parts of ADRC are not determined by the actual mathematic model of the system under control, but only affected by the range of its variation rate. Therefore, ADRC has robustness and adaptability against the external disturbance, variation of system parameters, and model changes.

III. ADRC for Induction Motor

Based on induction motor model that uses the rotor flux synchronous reference frame (d–q axis), the state space model of a squirrel case induction motor can be described by four nonlinear differential equations. Here, the q-axis rotor flux is equal to zero

$$\begin{cases} \dot{i}_{d1} = -k_1 i_{d1}+k_2\Psi_{d2}+i_{q1}\omega_1+\dfrac{1}{\sigma}u_{d1} & \text{(8a)}\\ \dot{\Psi}_{d2} = \dfrac{L_m}{T_r}I_{d1}-\dfrac{1}{T_r}\Psi_{d2} & \text{(8b)}\\ \dot{\omega}_r = k_3\Psi_{d2}i_{q1}-\dfrac{T_L n_p}{J} & \text{(8c)}\\ \dot{i}_{q1} = -k_1 i_{q1}-\dfrac{L_m}{\sigma L_r}\Psi_{d2}\omega_r-i_{d1}\omega_1+\dfrac{1}{\sigma}u_{q1} & \text{(8d)} \end{cases}$$

where

T_r	$\frac{L_r}{R_r}$;
σ	$L_s-\frac{L_m^2}{L_r}$;
k_1	$\frac{R_s L_r^2+R_r L_m^2}{\sigma L_r^2}$;
k_2	$\frac{R_r L_m}{\sigma L_r^2}$;
k_3	$\frac{n_p^2 L_m}{J L_r}$;
u_{d1},u_{q1}	d-axis (q-axis) stator voltage;

$$\begin{cases} \dot{z}_{11}=z_{12}\\ \vdots\\ \dot{z}_{1,n-1}=z_{1n}\\ \dot{z}_{1n}=-r\cdot(fal(z_{11}-v(t),\alpha,\delta)+b_1\cdot fal(z_{12},\alpha,\delta)+\cdots+b_{n-1}\cdot fal(z_{1n},\alpha,\delta)) \end{cases}$$
$$fal(\varepsilon,\alpha,\delta)=\begin{cases} |\varepsilon|^{\alpha}\operatorname{sign}(\varepsilon), & |\varepsilon|>\delta\\ \frac{\varepsilon}{\delta^{1-\alpha}} & |\varepsilon|\le\delta \end{cases} \tag{6}$$

i_{d1}, i_{q1}	d-axis (q-axis) stator current;
ψ_{d2}, ψ_{q2}	d-axis (q-axis) rotor flux;
ω_1	rotating speed of the coordinate;
ω_r	rotor angular speed;
T_L	load torque;
R_s, R_r	stator and rotor resistance;
L_s, L_r, L_m	stator, rotor, and mutual inductance;
J	rotor inertia;
n_p	pole pairs.

It is shown from the previous equations that

1) the system is nonlinear due to the coupled parts between state variables;
2) the performance of the whole system will be deteriorated by the variation of motor parameters and load conditions.

Here, it is assumed that $\omega_r, \psi_{d2}, i_{d1}, i_{q1}$, and their derivatives exist and are continuous. As it is shown in (8a)–(8d), the rotor flux loop is mainly controlled by (8a) and (8b) and the speed loop is affected mainly by (8c) and (8d). However, these two loops have some coupled parts, which could lead to sluggish dynamic response both in the speed loop and the flux loop.

In PID control scheme (shown in Fig. 1), the flux loop uses two PID controllers in cascade to control the rotor flux and d-axis current, the speed loop uses two PID controllers in cascade to control the rotor speed ω_r, and q-axis stator current i_{q1}. Reference [8] provided a method to design an optimal PID controller based on frequency domain analysis theory. It also considers the sampling delay as e^{-sT_s}, where T_s is the sampling period. This method is used to design the optimal PID controller for the induction motor control in this paper. The criterion is to achieve widest bandwidth and still maintain 50° phase margin. In the experiment, due to noises coupling and the parameter variation of the induction motors, the parameters have been refined. The following refined parameters are used both in the simulation and experiments. For the inner loop of speed subsystem $K_P = 40$, $K_I = 52\,000$, and $K_D = 0.003$. For the outer loop of speed subsystem $K_P = 13.5$, $K_I = 5100$, and $K_D = 0.001$. For the inner loop of flux subsystem $K_P = 40$, $K_I = 52\,000$, and $K_D = 0.003$. For the outer loop of flux subsystem $K_P = 230$, $K_I = 83\,000$, and $K_D = 0.015$.

In this paper, auto-disturbance rejection controllers (ADRC) are introduced to substitute the function of PID controllers to achieve high dynamic performance in the overall operating conditions (as shown in Fig. 3). As compared to the conventional PID scheme (as shown in Fig. 1), the control system includes two separate control loops: 1) the flux loop which uses one third-order ADRC to control the rotor flux and 2) the speed loop, which uses two second-order ADRC in cascade to control the rotor speed ω_r, and q-axis stator current i_{q1}, respectively. These controllers are robust against load and parameter disturbances. In addition, precise decoupling and linearization of induction motor is realized by using ADRC. Good torque/speed response can be maintained without precisely knowing the position and magnitude of rotor flux. Therefore, similar to direct torque control (DTC), the accurate flux observation in the control system is not required. This is one of the major advantages using ADRC into induction motor control.

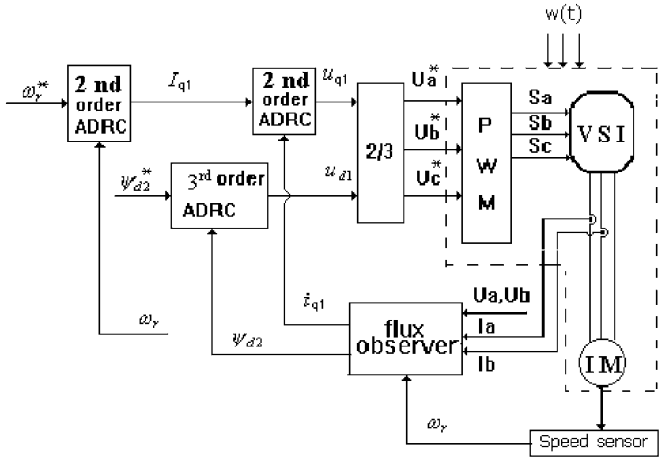

Fig. 3. Control system of induction motor using ADRC.

In this section, the application of ADRC into flux control loop is discussed in detail. By differentiating (8b), and combining with (8a), the secnd-order derivative of flux is derived as

$$\ddot{\psi}_{d2} = -\frac{1}{T_r}\dot{\psi}_{d2} + \frac{L_m}{T_r}k_2\psi_{d2} + \frac{L_m}{T_r}(-k_1 i_{d1} + i_{q1}\omega_1) + \frac{L_m}{T_r\sigma}u_{d1}. \quad (9)$$

As reported in (9), the third term $(L_m/T_r)(-k_1 i_{d1} + i_{q1}\omega_1)$ contains the information about the rotor speed, d-axis and q-axis current. In this term, the product of rotor speed and q-axis current $(L_m/T_r)i_{q1}\omega_1$ is the coupled part between flux loop and speed loop. This coupled part would deteriorate the control performance. If the whole third term $(L_m/T_r)(-k_1 i_{d1} + i_{q1}\omega_1)$ (including the coupled part $(L_m/T_r)i_{q1}\omega_1$) is regarded as the modeling uncertainty or internal disturbance of system, the following substitution is made:

$$\ddot{\psi}_{d2} = -\frac{1}{T_r}\dot{\psi}_{d2} + \frac{L_m}{T_r}k_2\psi_{d2} + w_{11}(t) + \frac{L_m}{T_r\sigma}u_{d1} \quad (10)$$

where $w_{11}(t) = (L_m/T_r)(-k_1 i_{d1} + i_{q1}\omega_1)$.

Equation (10) shows that the flux loop could be considered as a second-order subsystem. To control the rotor flux, a third-order ADRC is used. It is composed of three parts: 1) second-order nonlinear differentiator (ND), 2) third-order extended state observer (ESO), and 3) nonlinear state error feedback control law (NLSEF) (as shown in Fig. 4). Here, $w_1(t)$ represents the disturbances imposed on the flux subsystem. Their configurations are given in detail to illustrate how ADRC is used for induction motor control.

A. Second-Order ND for Flux Control

The flux loop is considered as a second-order subsystem, so second-order ND is used in the flux control loop (as shown in Fig. 4). It will arrange the flux transition process according to the input reference flux and the system under control. Its mathematic model is given as

$$\begin{cases} \dot{z}_{11} = z_{12} \\ \dot{z}_{12} = -r \cdot (fal(z_{11} - \psi^*_{d2}, \alpha, \delta) + b_1 \cdot fal(z_{12}, \alpha, \delta)) \end{cases} \quad (11)$$

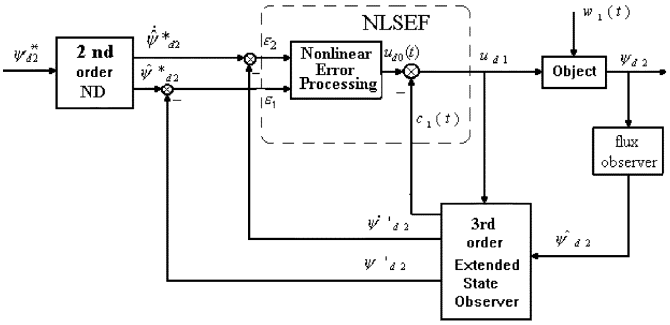

Fig. 4. Block diagram of third-order ADRC used in the flux control loop.

where ψ_{d2}^* is the given reference signal of rotor flux, $z_{11} = \hat{\psi}_{d2}^*$ and $z_{12} = \dot{\hat{\psi}}_{d2}^*$ are the arranged flux transition process and its derivative (shown in Fig. 4). Parameters r, α, δ, b_1, and function $fal(\varepsilon, \alpha, \delta)$ are defined in Section II-C2.

B. Third-Order ESO for Flux Control

In the flux control loop, a third-order ESO is utilized to achieve state and disturbance estimation (shown in Fig. 4). Its mathematic model is derived as

$$\begin{cases} \dot{z}_{21} = z_{22} - g_1(z_{21} - \hat{\psi}_{d2}) \\ \dot{z}_{22} = z_{23} - g_2(z_{21} - \hat{\psi}_{d2}) + \frac{L_m}{T_r\sigma}u_{d1} \\ \dot{z}_{23} = -g_3(z_{21} - \hat{\psi}_{d2}) \end{cases} \tag{12}$$

where $g_i(z_{21} - \hat{\psi}_{d2}) = \beta_i fal(z_{21} - \hat{\psi}_{d2}, \alpha, \delta)$, $i = 1, 2, 3$. $\hat{\psi}_{d2}$ is the observed flux by using flux observer and it is the input of ESO. $z_{21} = \psi'_{d2}$ and $z_{22} = \dot{\psi}'_{d2}$ are the estimated rotor flux and its derivative by using ESO (shown in Fig. 4). The third-order state of ESO z_{23} reveals the overall influence of modeling uncertainty $w_{11}(t)$. The definition of parameters β_i, α, δ, and function $fal(\varepsilon, \alpha, \delta)$ are all given in Section II-C1.

C. NLSEF for Flux Control

The NLSEF used in the flux control loop is to drive the rotor flux to the given reference flux. Its mathematical model is given as

$$u_{d0}(t) = k_1 fal(\varepsilon_1, \alpha, \delta) + k_2 fal(\varepsilon_2, \alpha, \delta) \tag{13}$$

$$u_{d1}(t) = u_{d0}(t) - c_1(t) \tag{14}$$

where $\varepsilon_1 = z_{11} - z_{21} = \hat{\psi}_{d2}^* - \psi'_{d2}$, $\varepsilon_2 = z_{12} - z_{22} = \dot{\hat{\psi}}_{d2}^* - \dot{\psi}'_{d2}$, $u(t) = u_o(t) - a(t)$, and z_{23} is the third-order state of ESO. The parameters k_1, k_2, α, δ, and function $fal(\varepsilon, \alpha, \delta)$ are defined in Section II-C3.

Similarly, when ADRC is applied to the speed control loop, the external load and the coupling part between the speed loop and flux loop can also be treated as internal disturbance. Therefore, (8c) and (8d) can be rewritten as

$$\begin{cases} \dot{\omega}_r = k_3\psi_{d2}i_{q1} + w_{21}(t) \\ \dot{i}_{q1} = -k_1 i_{q1} + w_{31}(t) + \frac{1}{\sigma}u_{q1} \end{cases} \tag{15}$$

where $w_{21}(t) = -T_L n_p/J$ represents the external load torque imposed on the system, and $w_{31}(t) = -(L_m/\sigma L_2)\psi_{d2}\omega_r - i_{d1}\omega_1$ is the coupled part between the flux and speed control subsystem.

In the speed subsystem, as shown in (15), the configuration of its control system is composed of two second-order ADRCs. One is used for speed regulation and another is used for q-axis current control (shown in Fig. 3). Their structure and mathematical model are all similar to that of flux subsystem. Here, two second-order ESOs are used to estimate the rotor speed, q-axis current, and their derivatives. The model uncertainties $w_{21}(t)$ and $w_{31}(t)$ are observed by the second-order states of ESO z_{22_w} and z_{22_s} separately.

According to the theory of ADRC [7], because the variation ranges of $w_{11}(t)$, $w_{21}(t)$, and $w_{31}(t)$ are finite, the external load disturbance and the coupled parts between the flux loop and speed loop can be completely estimated and compensated by ESO and NLSEF. Therefore, the dynamic equations of the whole system are simplified as

$$\begin{aligned} \ddot{\psi}_{d2} &= -\frac{1}{T_r}\dot{\psi}_{d2} + \frac{L_m}{T_r}k_2\psi_{d2} + \frac{L_m}{T_r\sigma}u_{d0} \\ \dot{\omega}_r &= k_3\psi_{d2}I_{q0} \\ \dot{i}_{q1} &= -k_1 i_{q1} + \frac{1}{\sigma}u_{q0} \end{aligned} \tag{16}$$

where u_{d0}, I_{q0}, and u_{q0} are the control signals before compensation, and the given control signals after compensation can be defined as

$$u_{d1} = u_{d0} - \frac{z_{23}(t)}{\frac{L_m}{(T_r\sigma)}} \tag{17}$$

$$I_{q1} = I_{q0}\frac{-z_{22\_w}(t)}{(k_3\psi_{d2})} \tag{18}$$

$$u_{q1} = u_{q0} - z_{22\_s}(t)\cdot\sigma. \tag{19}$$

Here, $(z_{23}(t))/(L_m/(T_r\sigma))$, $z_{22\_w}(t)/(k_3\psi_{d2})$, and $z_{22\_s}(t)\cdot\sigma$ are considered to be correction or compensation items. They are estimated by ESO, and then compensated by NLSEF separately.

It can be seen that due to the compensation made by NLSEF [shown in (17)–(19)], the whole system of the induction motor is simplified as (16). There is no coupled part between the flux control subsystem and speed control subsystem. The impact of external load disturbances is also eliminated. Therefore, the decoupling of the rotor flux and speed control loop is achieved. Furthermore, this dynamic feedback linearization method doesn't need the actual expression of the mathematical model of induction motors. The robustness and adaptability of the control system is significantly improved.

As it is mentioned above, the dynamic model of the induction motor is precisely decoupled into two linear subsystems: 1) flux subsystem and 2) speed subsystem (shown in Fig. 5). It is obvious from Fig. 5, that the precise decoupling of flux/speed control and exact linearization can be achieved if ESO achieves the state and model disturbance estimation accurately. So, it is convenient to use a third-order ADRC to give out the flux control signal u_{d1}, and use two second-order ADRC in cascade to send out the speed and current control signal i_{q1} and u_{q1} separately [9] (shown in Fig. 3).

{It is observed, that rotor resistor and load torque changes most frequently when the induction motor is operating. For the ADRC presented in this paper, only the variation of rotor resistance and load torque are considered. Nevertheless, ADRC can

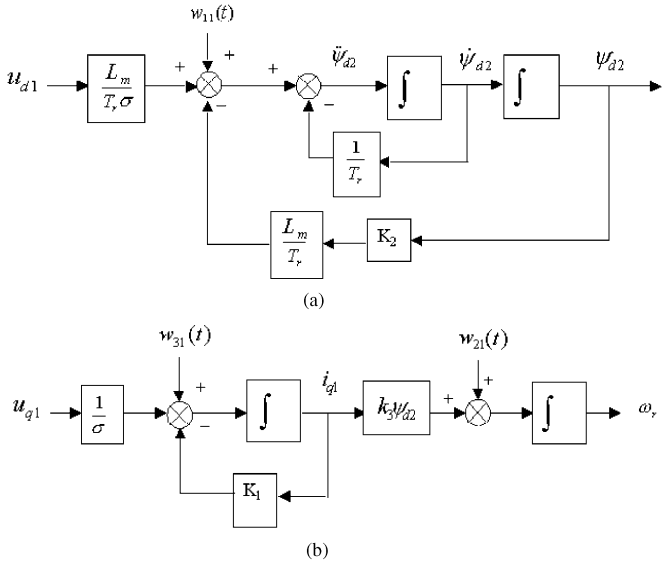

Fig. 5. Equivalent dynamic mathematical model of induction motor (a) flux subsystem and (b) speed subsystem.

also be used to compensate the variation of other parameters. Then, (10) (15) can be rewritten

$$\ddot{\psi}_{d2} = -\frac{1}{T_r}\dot{\psi}_{d2} + \frac{L_m}{T_r}k_2\psi_{d2} + w_{11}(t) + \frac{L_m}{T_r\sigma}u_{d1} + w_{12}(t)$$

$$w_{12}(t) = \left(\frac{1}{T_r} - \frac{1}{T_r}\right)\dot{\psi}_{d2} + \left(\frac{L_m}{T_r}k_2 - \frac{L_m}{T_r}k_2\right)\psi_{d2} + \left(\frac{L_m}{T_r\sigma} - \frac{L_m}{T_r\sigma}\right)u_{d1} \quad (20)$$

$$\begin{cases} \dot{\omega}_r = k_3\psi_{d2}i_{q1} + w_{21}(t) + w_{22}(t) \\ \dot{i}_{q1} = -k_1 i_{q1} + w_{31}(t) + \frac{1}{\sigma}u_{q1} + w_{32}(t) \end{cases} \quad (21)$$

where $w_{22}(t) = \Delta T_L \cdot n_p/J$, $w_{32}(t) = (k_1 - k_1') \cdot i_{q1}$, and T_r', k_1', and k_2' are the induction motor coefficients when rotor resistant is changed. ΔT_L is the load torque change.

Based on (20) and (21), the external load change and internal parameter variation are all treated as disturbances imposed on the controlled system. Due to the fact that the variation range of load and parameter change is finite, then by properly selecting the functions and related parameters of ESO and NLSEF, we can accurately estimate and compensate the overall influence of parameter variation and external disturbance. These functions and parameters of ADRC are all independent of the object under control. Therefore, the closed loop motor drive system under ADRC control does not depend on the accurate mathematical model of induction motors. It has good robustness and adaptability to parameter variation and load disturbance. This is the chief reason why ADRC is utilized here. In Appendix B, the function of the ADRC parameters are analyzed and the method to adjust the parameters of ADRC is given. In Appendix C, all the values of ADRC parameters for the induction motor control used in this paper are listed.

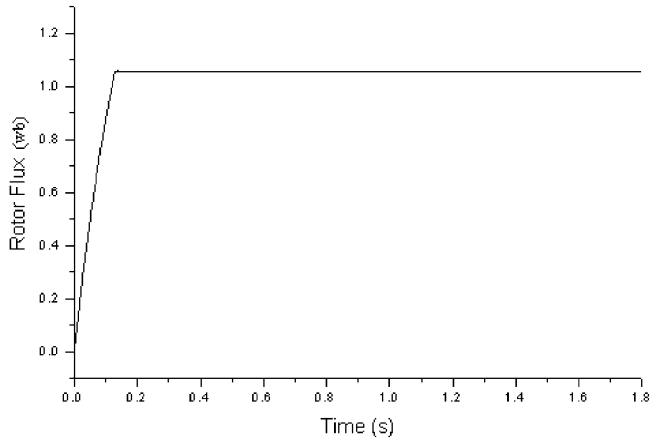

Fig. 6. Rotor flux dynamic response during startup by using ADRC.

IV. Simulation and Experimental Results

Computer simulation and experiments were conducted to evaluate the performance of the proposed ADRC by using a three-phase 2.2-kW induction motor. The parameters of the induction motor are listed as

$$Rs = 2.92\,\Omega \quad Rr = 1.92\,\Omega \quad Ls = 0.371\text{ H}$$
$$\text{Lr} = 0.371\text{ H} \quad Lm = 0.358\text{ H} \quad \text{Polepairs} = 2$$
$$J = 0.1\text{ kg}\cdot\text{m}^2 \quad \text{Rated Speed} = 1430\text{ rpm}.$$

A. Simulation Results

All simulations were done with a load torque change applied to the induction motor. The program language for simulation is C++. To see the influence of the proposed controller, the performances of ADRC and conventional PID controller were compared under the same conditions.

Fig. 6 shows the startup waveform of the rotor flux. The reference of rotor flux is set to be 1.05. It is demonstrated that by using third-order ADRC, the rotor flux is successfully controlled. Fig. 7(a) shows the actual and estimated rotor angular speed ω_r during startup and load change. At $t = 1.1$ s, load torque $T_L = 15\text{ N}\cdot\text{m}$ is applied to the induction motor. Compared to the steady-state value of rotor speed, the speed change caused by load disturbance is very small. Therefore, it is not obvious in Fig. 7(a). Fig. 7(b) shows the derivative of rotor angular speed including the actual value and the value estimated by ESO. The simulation traces show that there is almost no difference between the observed values and its reference signals. These figures indicate that the extended state observer can successfully track the state variables of the induction motor and their derivatives.

Fig. 8 shows the dynamic responses of ADRC and PID controller at rated speed. A step load change $T_L = 15\text{ N}\cdot\text{m}$ is applied to the induction motor at $t = 1.1$ s. By using ADRC, the speed response shows no overshoot and it settles down quickly to a steady-state without any steady-state error. In addition, under the control of ADRC, the peak value of speed vibration (1.5 rpm) due to sharp change of load torque is smaller than that of the conventional PID controller (1.8 rpm). The

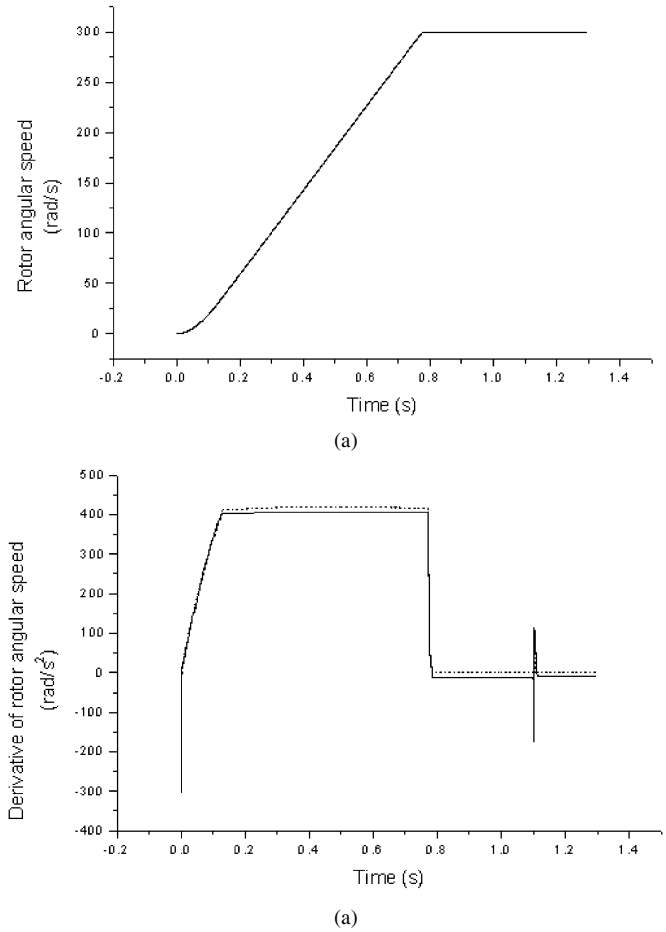

Fig. 7. (a) Actual (solid line) and estimated (dashed line) rotor angular speed. (b) Actual (solid line) and estimated (dashed line) rotor angular speed derivative.

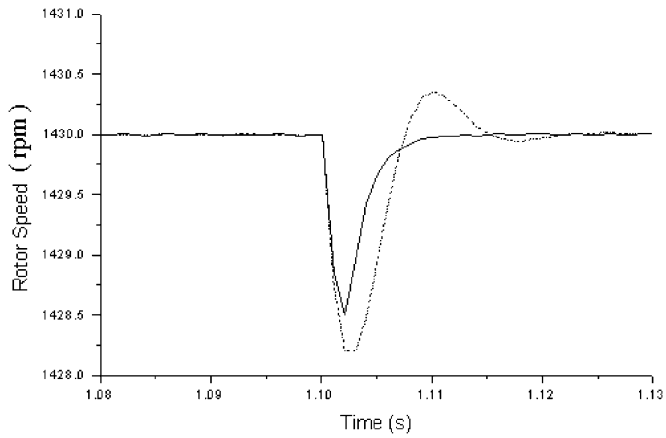

Fig. 8. Dynamic responses of ADRC (solid line) and PID controller (dashed line) due to load torque change (from 0–15 N · m) at rated speed.

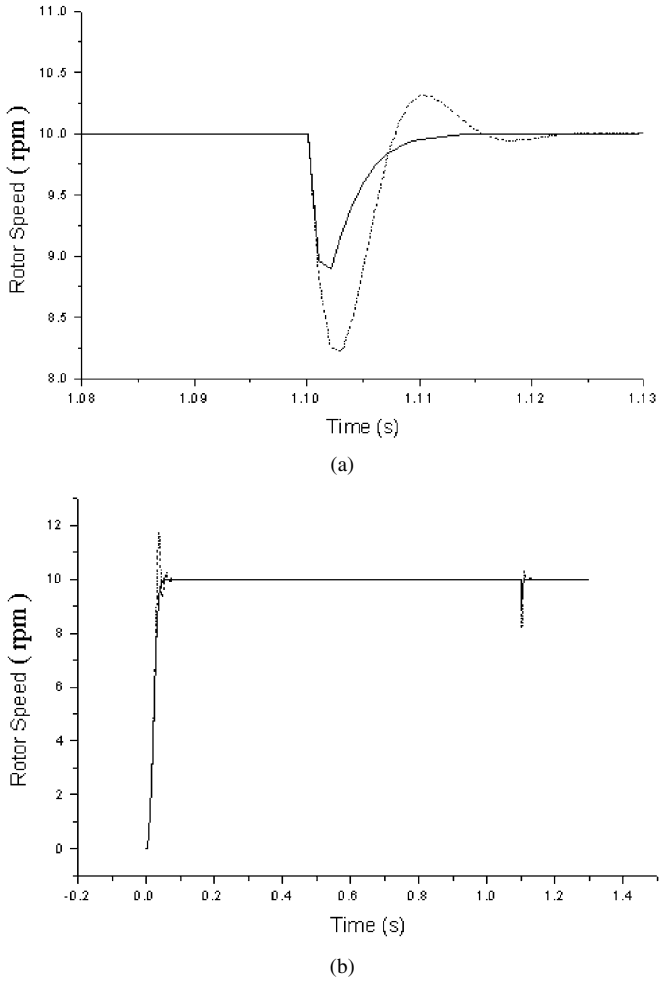

Fig. 9. (a) Dynamic responses of speed regulation at low speed (10 rpm)—Using ADRC (solid line); Using PID controller (dashed line). (b) Startup curve of rotor speed at low speed setting (10 rpm)—Using ADRC (solid line); Using PID controller (dashed line).

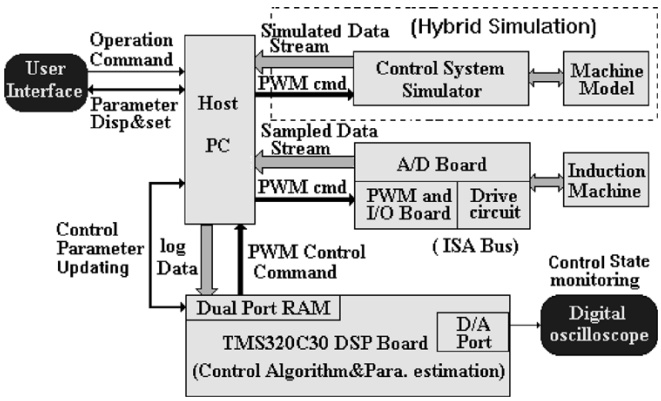

Fig. 10. Configuration of experimental setup (dual-CPU flexible control system).

setting time of ADRC (0.01 s) is smaller than that of the PID controller (0.02 s) as well. All of these results verify that by using ADRC, the estimation and compensation of the impact of load disturbance is implemented efficiently and no integration operation is needed.

In order to evaluate the dynamic performance of ADRC under a wide operation range, the parameters of the ADRC and PID controller have been optimized at rated speed (1430 rpm). Then, the same controllers are applied to regulate the induction motor at low speed (10 rpm) without changing their parameters. A step load change $T_L = 15$ N · m is applied to the induction motor at $t = 1.1$ s. By comparing Figs. 8 and 9(a), we can see that under different operating conditions, ADRC can still maintain its excellent dynamic performance, such as fast response time, no overshoot, and robustness to load disturbances. So it

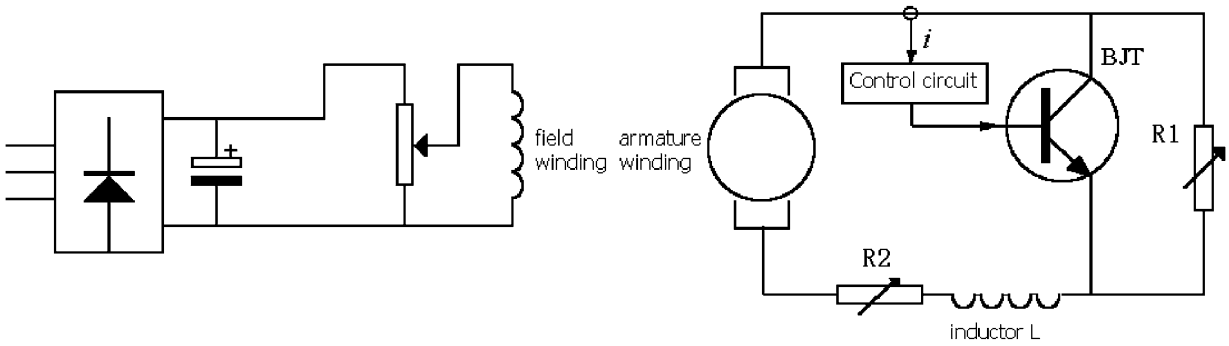

Fig. 11. Implementation of the load for induction motor.

doesn't need to adjust the parameters of ADRC for different operating points. From Fig. 9(b), we can see that by using PID controller, the startup curve at low speed setting is worse than that of ADRC. The overshoot occurs and the settling time is longer as compared with that of ADRC. But by using ADRC, it maintains its good startup characteristics (fast and no overshoot) both at high and low speed [as shown in Figs. 7(a) and 9(b)].

B. Experimental Results

A prototype was built for the same induction motor and controller parameters as used in the simulations. In order to verify the dynamic performance of the designed ADRC, experiments were performed on the dual-CPU flexible control system (shown in Fig. 10). The cores of the control system are a host personal computer (PC) and a TMS320C30 DSP development board. The user interface, PWM pulse generation, and A/D data acquisition were controlled by the host PC. The DSP deals with the control algorithm, parameter estimation, and state observation. The host PC transfers the feedback data such as the sensed current, voltage, and rotor speed to the DSP through the dual-port RAM. The C30DSP processes the data from the dual-port RAM and returns the PWM control commands back. In the experimental implementation, the required time for the DSP to execute all the tasks is approximately 160 μs. The switching frequency of the PWM signal is 5 kHz. The A/D board is designed with AD7874 12-b chips, which integrate sample and hold circuits and an analog multiplexer (MUX). A 4 K 16-b FIFO buffer was used to help the PC in importing the sampled data. In this paper, a dc generator is used as the load of the induction motor (shown in Fig. 11). The field current of the dc generator is constant. The load torque can be changed by changing the armature resistor. Using this circuit, the torque will be kept constant when the induction motor rotates in the positive direction. Unfortunately, due to the limitation of this load system, the load torque is proportional to its rotating speed when the induction motor rotates in the negative direction. This causes the asymmetries in ADRC performance shown in Fig. 16(a). It should be noted that if a proper load system is used, there will be no asymmetries as shown in Fig. 16(a).

Figs. 12 and 13 show the speed response curves of the induction motor with load torque $T_L = 6\,\mathrm{N}\cdot\mathrm{m}$ while the setting rotor speed is changed. In Fig. 12, at $t = 0.65$ s, the setting speed is changed to 240 rpm, and at $t = 2.25$ s the setting speed is changed back to 120 rpm. In Fig. 13, at $t = 0.65$ s, the setting speed is changed to -120 rpm, and at $t = 1.95$ s, the setting speed is changed back to 120 rpm. The chatting in the speed response of PID controller (shown in Fig. 13) is due to the fact that its tuning is dependent on parameters and conditions. It could not work well under different operation conditions without modifying its parameters. For ADRC, it can precisely monitor the variation tendency of rotor speed and compensate it in advance. As a result, it achieves better dynamic performance and adaptability than a PID controller over wide speed range.

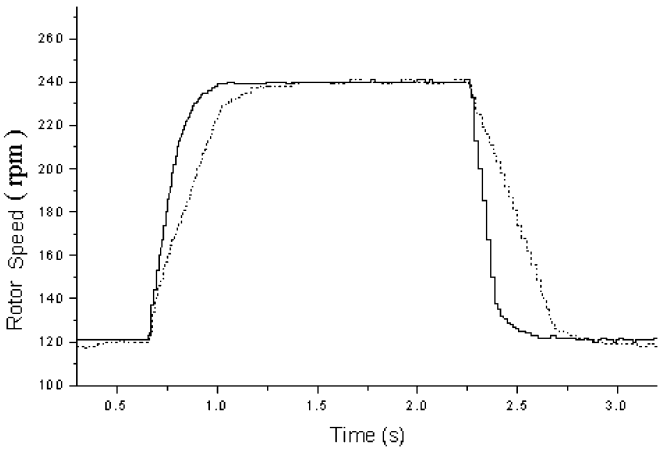

Fig. 12. Dynamic speed responses of induction motor (changed from 120 to 240 rpm)—ADRC (solid line); PID controller (dashed line).

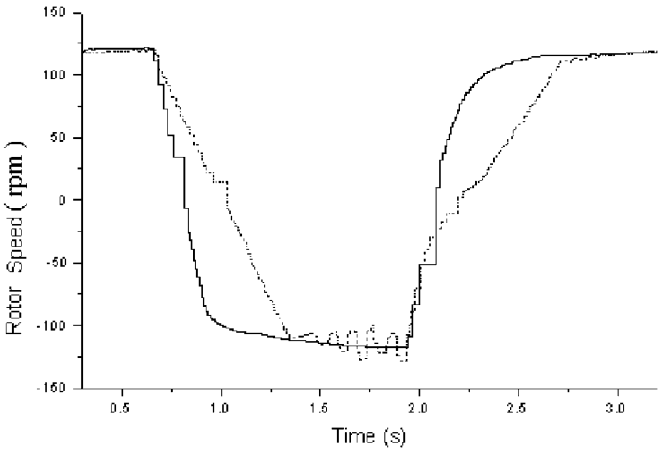

Fig. 13. Dynamic speed responses of induction motor (changed from 120 to -120 rpm)—ADRC (solid line); PID controller (dashed line).

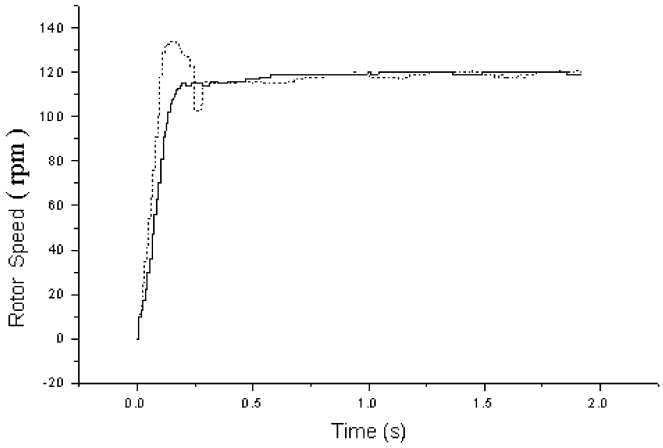

Fig. 14. Startup curve of the induction motor when the given rotor resistant is changed to 1.0 Ω (original value: 1.92 Ω)—ADRC (solid line); PID controller (dashed line).

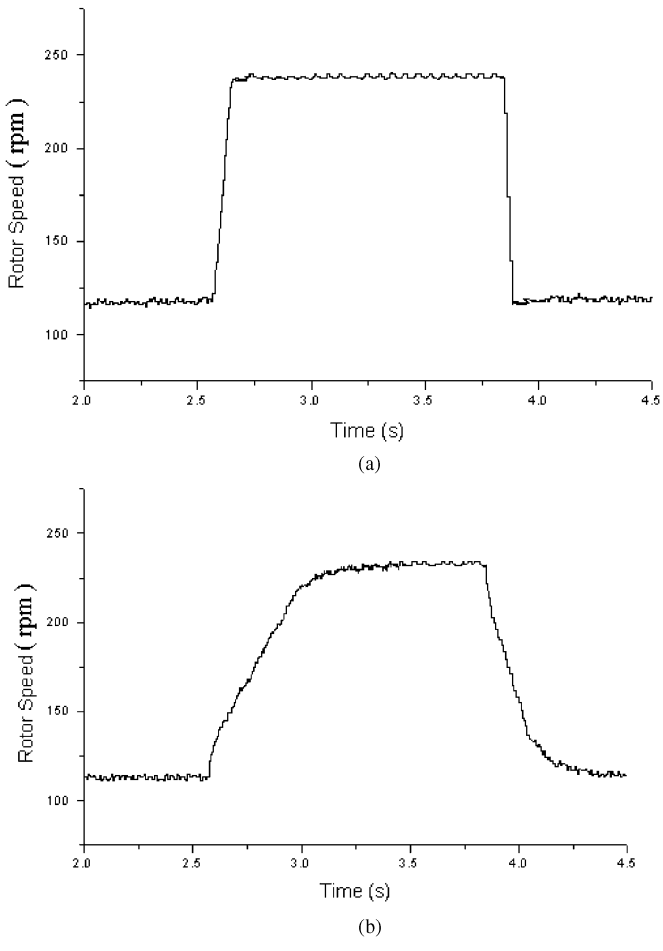

Fig. 15. Dynamic speed responses of induction motor from 120 to 240 rpm when the given rotor resistant is changed to 1.0 Ω (original value: 1.92 Ω). (a) ADRC. (b) PID controller.

As mentioned before, the variation of motor parameters may have great influence on the control system performance. In order to verify the robustness of ADRC under parameter variations, the rotor resistor changes are imitated by resetting the value of given rotor resistance in the model of the induction motor

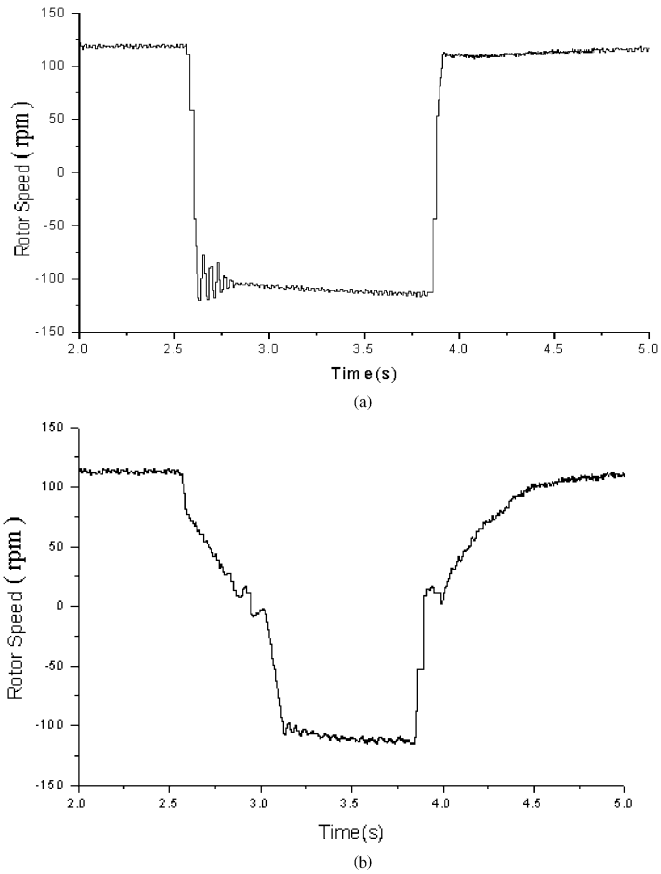

Fig. 16. Dynamic speed responses of induction motor from 120 to -120 rpm when the given rotor resistant is changed to 1.0 Ω (original value: 1.92 Ω). (a) ADRC. (b) PID Controller.

to be approximately 50% lower (from 1.92 to 1.0 Ω) or 25% higher (from 1.92 to 2.5 Ω) than that of the actual rotor resistance, respectively. All these rotor resistance values of induction motor have been reset before the induction motor starts up. After that, we operate ADRC and PID controller under the same working situations. In Fig. 14, we can see that ADRC can maintain much better dynamic performance than that of PID controller such as no overshoot and small transient time during startup. Figs. 15–18 show the dynamic speed response of inductor motor using ADRC and conventional PID controller when the given rotor resistance is changed. In Figs. 15 and 17, at $t = 2.6$ s, the setting speed is changed to 240 rpm, and at $t = 3.85$ s, the setting speed is changed back to 120 rpm. In Figs. 16 and 18, at $t = 2.6$ s, the setting speed is changed to -120 rpm, and at $t = 3.85$ s, the setting speed is changed back to 120 rpm. It can be seen that the dynamic performance of PID controller changes at different rotor resistant settings. Under some operating conditions, the dynamic performance of the PID controller deteriorates significantly, its transient time prolonged, and some oscillation emerges during acceleration and deceleration. At the same time, ADRC can still maintain good speed regulation in spite of parameter changes. From these figures, it can be noted that ADRC can achieve robustness and adaptability to external and internal disturbances. Its dynamic performance is better than that of PID controller under all operating conditions and different system parameters.

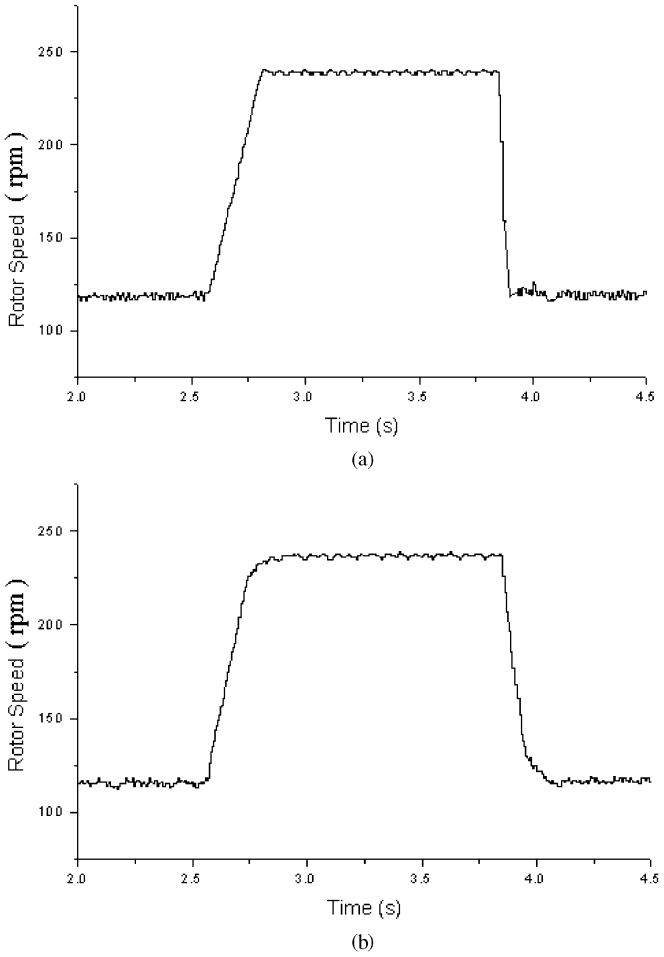

Fig. 17. Dynamic speed responses of induction motor from 120 to 240 rpm when the given rotor resistant is changed to 2.5 Ω (original value: 1.92 Ω). (a) ADRC. (b) PID Controller.

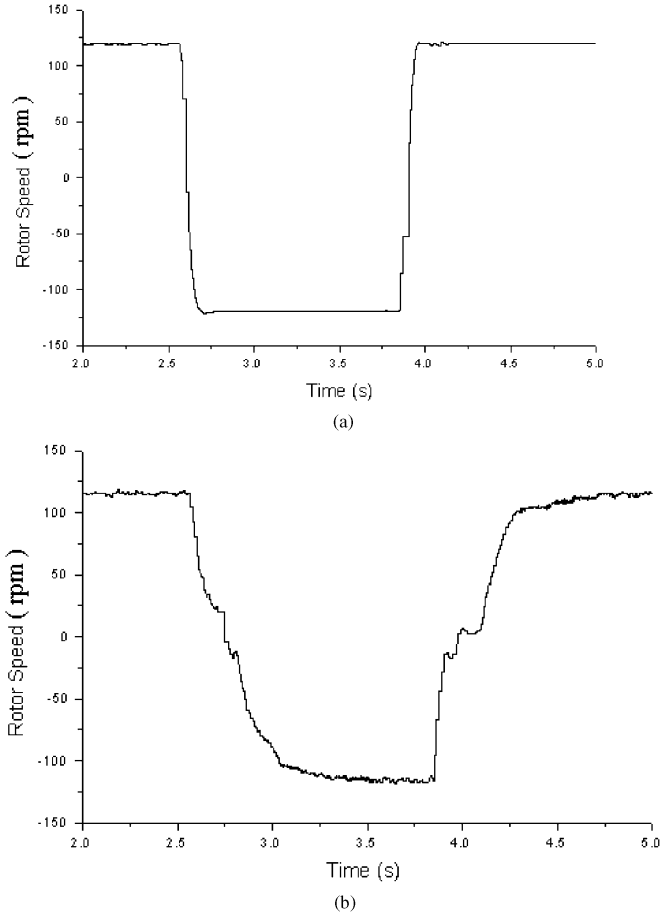

Fig. 18. Dynamic speed responses of induction motor from 120 to -120 rpm when the given rotor resistant is changed to 2.5 Ω (original value: 1.92 Ω). (a) ADRC. (b) PID Controller.

V. Conclusion

In this paper, the auto disturbance rejection controller (ADRC) has been applied to the induction motor control. The basis of ADRC is the extended state observer and nonlinear feedback control. The state estimation and compensation of the change of motor parameters and load variations are implemented by ESO and NLSEF. By using ESO, the complete decoupling of the induction motor is obtained. The generalized derivatives of given signals are achieved accurately. The major advantage of the proposed method is that the closed loop characteristics of the motor drive system do not depend on the exact mathematical model of the induction motor. Comparisons were made in detail between ADRC and conventional PID controller.

It is concluded that the proposed control algorithm produces better dynamic performance than the PID controller. As verified with simulation and experimental results, the proposed ADRC control system is robust against the modeling uncertainty and the external disturbance in various operating conditions. These results open new perspectives on utilization of nonlinear topologies on vector control. It is indicated that such scheme can be applicable to industrial application where high dynamic performance is required.

Appendix A
Steady-State Error Analysis

This appendix analyzes the steady-state error for linear control systems and nonlinear control systems. In the second example of Section II-B, a first-order system $\dot{x} = -cx + u$ is used. Without losing generality, it can be assumed that $c > 0$ and the reference value of x is v, where v is constant and $v > 0$.

By using the linear feedback control $u = k(v - x(t))$, where $k > 0$, in the steady-state, $\dot{x} = 0$. Then, it can be understood that $x = (k/(c+k))v$.

Therefore, the steady-state error e_{linear} under linear feedback $u = k(v - x(t))$ is

$$e_{\text{linear}} = v - x = \frac{c}{c+k}v. \tag{A1}$$

From (A1), it can be seen that

$$e_{\text{linear}} \approx \frac{c}{k}v \text{ if } c \ll k. \tag{A2}$$

For the nonlinear feedback $u = k|v - x(t)|^{\alpha}\text{sign}(v - x(t))$, $0 < \alpha < 1$, k is chosen to be the same value as that used in the linear feedback.

Without losing generality, we can assume that in the steady-state, $0 < x < v$ and the steady-state error under nonlinear feedback control, is $e_{\text{nonlinear}} = v - x > 0$. Otherwise, if in the steady-state, $0 < v < x$, from the function $\dot{x} = -cx + u =$

$-cx - k|v - x(t)|^{\alpha}$, then it is understood that at this condition $\dot{x} < 0$. The system will be in the dynamic transients again.

In the steady-state $\dot{x} = 0$. Then

$$k(v - x)^{\alpha} = cx. \tag{A3}$$

Dividing both sides of (A3) by v^{α}, the following equation can be derived:

$$k\left(1 - \frac{x}{v}\right)^{\alpha} = \frac{cx}{v^{\alpha}}. \tag{A4}$$

When considering $0 < x < v$, (A4) can be rewritten as

$$k\left(1 - \frac{x}{v}\right)^{\alpha} = \frac{cx}{v^{\alpha}} = c \cdot \left(\frac{x}{v}\right) \cdot v^{1-\alpha} < cv^{1-\alpha}. \tag{A5}$$

By rearranging (A5), the following relation can be derived:

$$\left(1 - \frac{x}{v}\right) < \left(\frac{c}{k}\right)^{(1/\alpha)} v^{((1-\alpha)/\alpha)}. \tag{A6}$$

Multiply both sides of (A6) by v, the relation of steady-state error under nonlinear control can be derived as:

$$e_{\text{nonlinear}} = v - x < \left(\frac{c}{k}\right)^{(1/\alpha)} \cdot v^{(1/\alpha)}. \tag{A7}$$

Comparing (A2) and (A7), it can be observed that if $c \ll k$, $cv \ll k$, and $0 < \alpha < 1$

$$\frac{e_{\text{nonlinear}}}{e_{\text{linear}}} < \left(\frac{cv}{k}\right)^{(1/\alpha)-1}. \tag{A8}$$

For example, if $(cv/k) = 0.01$, and $\alpha = (1/2)$, then $e_{\text{linear}} \approx 0.01$, $e_{\text{nonlinear}} < 0.01^2 = 0.0001$, and $(e_{\text{nonlinear}}/e_{\text{linear}}) < 0.01$.

The previous analysis verifies that if k is selected large enough, by using nonlinear feedback, the steady error of the system is much less than that of using linear feedback.

APPENDIX B
ADJUSTMENT OF THE ADRC PARAMETERS

The parameters of ADRC have a big influence on the dynamic performance of the controlled system. Therefore, it is very important to adjust these parameters properly. In this appendix, the method to adjust the parameters of ADRC used in this paper is given. For simplicity, the flux control loop is used as an example. The adjustment methods for the other loops are the same.

A. Adjustment of Nonlinear Differentiator (ND)

The parameter modification of ND is for the purpose of optimizing the design trade off between fast transit process and overshoot. The parameters of ND which determine its performance are r, b_1, α, and δ [shown in (11)]. r is the converge rate coefficient and is regulated according to the required dynamic response time. The larger the r is, the faster z_{11} converges to ψ_{d2}^{*}. However, if r is too large, the noise in the signal will impact the robustness of the controller. Furthermore, if r is too large, the function of defining transient response profile will be lost, and the output of ND will be almost the same as its input signal. Therefore, it cannot solve the conflict between fast response and no overshoot. As a result, r should satisfy the conditions that for the given step signal in the input, its output signal is continuous, smooth, and its derivative is finite. b_1 is the fine tuning factor of ND. It affects the converge speed of z_{12}.

δ in (11) is the width of linear area in the nonlinear function of ND. It plays an important role to the dynamic performance of ND. The larger the δ is, the wider the linear area. But if the δ is too large, the benefit of nonlinear characteristics would be lost. On the other hand, if δ is too small, high frequency chatting will happen just the same as in the sliding mode control. Generally, in ND, δ is set to be approximately 10% of the variation range of its input signal.

α is the exponent of tracking error. In order to decrease the calculation time in real-time implementation, α is set to be equal to $\alpha = (m/2^n)$, $n = 1, 2, \ldots$, and $m \leq 2^n$. The smaller the α, the faster the tracking speed, but the more calculation time is needed. In addition, very small α will cause chatting. In reality, selecting $\alpha = 1/2$ will provide a satisfactory result.

B. Adjustment of Extended State Observer (ESO)

It can be observed from (12), that the structure of ESO is mainly based on the switching functions $g_i(z_{21} - \hat{\psi}_{d2}) = \beta_i fal(z_{21} - \hat{\psi}_{d2}, \alpha, \delta)$. The role and regulation method of α and δ are similar to those in nonlinear differentiator. In the simulation and experiment, it is found that if the functions of ESO are selected as $g_i(z_{21} - \hat{\psi}_{d2}) = \beta_i \cdot (z_{21} - \hat{\psi}_{d2})$ $(i = 1, 2, \ldots, n)$ and $g_{n+1}(z_{21} - \hat{\psi}_{d2}) = \beta_{n+1} \cdot fal(z_{21} - \hat{\psi}_{d2}, \alpha, \delta)$ $(0 < \alpha < 1)$, the system can maintain good dynamic performance. At the same time, the calculation time is significantly decreased (this means for function $g_i(z_{21} - \hat{\psi}_{d2})$ $(i < n + 1)$, $\alpha = 1$, and $\delta = 1$). For $g_{n+1}(z_{21} - \hat{\psi}_{d2})$, δ is set to be approximately 1% of the variation range of its input signal and α is set to be 1/2.

Different to nonlinear differentiator, the estimation speed of rotor flux and its derivatives are mainly influenced by β_i $(i = 1, 2, \ldots, n)$. The larger β_1 is, the faster z_{21} converges to $\hat{\psi}_{d2}$. The larger the β_2 is, the faster z_{22} converges to $\dot{\hat{\psi}}_{d2}$. The larger the β_3 is, the faster z_{23} converges to $\ddot{\hat{\psi}}_{d2}$. However, if β_i is too large, the robustness against the noises will be deteriorated. In addition, β_1 is also affected by sampling frequency fs of the control system. In general, β_1 is set to be one to four times that of the sampling frequency fs, $\beta_2 > 10\beta_1$, and $\beta_3 > 10\beta_2$. By choosing $\beta_{i+1} \gg \beta_i$ $(i = 1, 2, \ldots, n)$, higher order state observation $z_{2,i+1}$ will converge to the actual value more quickly than lower order state observation z_{2i}. Therefore, the stability of ADRC system will be guaranteed.

C. Adjustment of Nonlinear State Error Feedback Control Law (NLSEF)

It can be observed from (13), that the response speed of the flux loop can be regulated by k_1 and k_2. Increasing k_1 and k_2 will speed up the system response. Similarly, care should be

taken to ensure that k_1 and k_2 should not be too large in order to avoid overshoot. The role and regulation method of α and δ in NLSEF are similar to that in ESO.

D. Some Notes

It should be noted that ADRC is a highly nonlinear structure. Its parameters, including exponent parameter α, the linear area width δ, and other parameters such as r β, and k, all affect the performance of ADRC. At the present time, there are no good rules/methods to determine the parameters for nonlinear controllers and linear controllers.

The parameter selection method proposed in this appendix is only a starting point. The performance of the ADRC system can be further improved by adjusting these parameters using computer simulations and/or experimental prototypes. Usually, in most cases, the final numbers of the ADRC parameters are close to the selected number by using the parameter selection method proposed in this appendix.

APPENDIX C
ADRC PARAMETER VALUES

In this appendix, all the values of ADRC parameters for the induction motor control used in this paper are listed.

A. Flux Subsystem

The ADRC used in flux subsystem is composed of a second-order ND, a third-order ESO, and a second-order NLSEF. Their constructions are listed as follows.

1) ND

$$\begin{cases} \dot{z}_{11} = z_{12} \\ \dot{z}_{12} = -r \cdot (fal(z_{11} - \psi_{d2}^*, \alpha, \delta) + b_1 \cdot fal(z_{12}, \alpha, \delta)) \end{cases}$$

where ψ_{d2}^* is the given reference signal of rotor flux. $r = 2 * 10^6$, $b_1 = 0.03$, $\alpha = 1/2$, and $\delta = 0.1$.

2) ESO

$$\begin{cases} \dot{z}_{21} = z_{22} - g_1(z_{21} - \hat{\psi}_{d2}) \\ \dot{z}_{22} = z_{23} - g_2(z_{21} - \hat{\psi}_{d2}) + \frac{L_m}{T_r \sigma} u_{d1} \\ \dot{z}_{23} = -g_3(z_{21} - \hat{\psi}_{d2}) \end{cases}$$

where $g_i(z_{21} - \hat{\psi}_{d2}) = \beta_i fal(z_{21} - \hat{\psi}_{d2}, \alpha, \delta)$.
For $g_1(z_{21} - \hat{\psi}_{d2})$, $\alpha = 1$, $\delta = 1$, and $\beta_1 = 18\,000$.
For $g_2(z_{21} - \hat{\psi}_{d2})$, $\alpha = 1$, $\delta = 1$, and $\beta_2 = 9 * 10^7$.
For $g_3(z_{21} - \hat{\psi}_{d2})$, $\alpha = 1/2$, $\delta = 0.01$, and $\beta_3 = 1 * 10^9$.

3) NLSEF

$$u_0 = k_1 fal(\varepsilon_1, \alpha, \delta) + k_2 fal(\varepsilon_2, \alpha, \delta)$$
$$\varepsilon_1 = z_{11} - z_{21}, \quad \varepsilon_2 = z_{12} - z_{22}$$
$$u_{d1}(t) = \frac{u_0(t) - z_{23}}{\left(\frac{L_m}{T_r \sigma}\right)}$$

where $\alpha = 3/4$, $\delta = 0.01$, $k_1 = 5000$, and $k_2 = 1$.

B. Speed Subsystem

The control configuration of speed subsystem is composed of two second-order ADRC. One is used for speed regulation and another is used for q-axis current control.

1) Speed Control Loop:

a) ND

$$\dot{z}_{11} = -r fal(z_{11} - \omega_r^*, \alpha, \delta)$$

where ω_r^* is the given reference signal of rotor speed. $r = 3800$, $\alpha = 1/2$, and $\delta = 10$.

b) ESO

$$\begin{cases} \dot{z}_{21} = z_{22} - g_1(z_{21} - \omega_r) + k_3 \psi_{d2} I_{q1} \\ \dot{z}_{22} = -g_2(z_{21} - \omega_r) \end{cases}$$

where $g_i(z_{21} - \omega_r) = \beta_i fal(z_{21} - \omega_r, \alpha, \delta)$ $(i = 1, 2)$, and I_{q1} is the reference signal of q-axis current.
For $g_1(z_{21} - \omega_r)$, $\alpha = 1$, $\delta = 1$, and $\beta_1 = 18\,000$.
For $g_2(z_{21} - \omega_r)$, $\alpha = 1/2$, $\delta = 0.5$, and $\beta_2 = 8 * 10^7$.

c) NLSEF

$$u_0 = k_1 fal(\varepsilon_1, \alpha, \delta)$$
$$I_{q1}(t) = \frac{u_0(t) - z_{22}}{(k_3 \psi_{d2})}$$

where $\varepsilon_1 = z_{11} - z_{21}$, $\alpha = 3/4$, $\delta = 0.5$, and $k_1 = 10$

2) q-Axis Current Control Loop:

a) ND

$$\dot{z}_{11} = -r fal(z_{11} - I_{q1}, \alpha, \delta)$$

where $r = 10\,000$, $\alpha = 1/2$, and $\delta = 20$.

b) ESO

$$\begin{cases} \dot{z}_{21} = z_{22} - g_1(z_{21} - i_{q1}) + \frac{1}{\sigma} u_{q1} \\ \dot{z}_{22} = -g_2(z_{21} - i_{q1}) \end{cases}$$

where $g_i(z_{21} - i_{q1}) = \beta_i fal(z_{21} - i_{q1}, \alpha, \delta)$ $(i = 1, 2)$.
For $g_1(z_{21} - i_{q1})$, $\alpha = 1$, $\delta = 1$, and $\beta_1 = 5000$.
For $g_2(z_{21} - i_{q1})$, $\alpha = 1/2$, $\delta = 2$, and $\beta_2 = 3 * 10^6$.

c) NLSEF

$$u_0 = k_1 fal(\varepsilon_1, \alpha, \delta)$$
$$u_{q1}(t) = \frac{u_0(t) - z_{22}}{\left(\frac{1}{\sigma}\right)}$$

where $\varepsilon_1 = z_{11} - z_{21}$, $\alpha = 3/4$, $\delta = 2$, and $k_1 = 80$.

REFERENCES

[1] R. S. Cabrera and J. Morales, "Some results about the control and observation of induction motors," in *Proc. IEEE American Control Conf.*, vol. 3, 1995, pp. 1633–1637.

[2] Y. Ping, D. Vrancic, and R. Hanus, "Anti-windup, bumpless, and conditioned transfer techniques for PID controllers," *IEEE Trans. Control Syst. Technol.*, vol. 16, pp. 48–57, Aug. 1996.

[3] K. J. Astrom and T. Hagglund, *Automatic Tunning of PID Controllers*. Research Triangle Park, NC: Instrum. Soc. Amer., 1988, pp. 3–28.

[4] N. J. Krikelis and S. K. Barkas, "Design of tracking systems subject to actuator saturation and integral wind-up," *Int. J. Control*, vol. 39, no. 4, pp. 667–682, 1984.

[5] J. Chen and Y. Li, "Virtual vectors based predictive control of torque and flux of induction motor and speed sensorless drives," in *Proc. IEEE 34th Industrial Applications Soc. Annu. Meeting*, vol. 4, 1999, pp. 2606–2613.

[6] C. Cecati and G. Guidi, "An adaptive nonlinear control algorithm for induction motor," in *Proc. IEEE Annu. Conf. Industrial Electronics Soc.*, vol. 1, 1996, pp. 326–331.

[7] J. Han, "Auto-disturbances-rejection controller and its applications," *Trans. Control Dec., China*, vol. 13, no. 1, pp. 19–23, 1998.

[8] B. C. Kuo, *Automatic Control Systems*, Sixth ed. Englewood Cliffs, NJ: Prentice-Hall, 1991, pp. 665–679.

[9] G. Feng, L. Huang, and D. Zhu, "A nonlinear auto-disturbance rejection controller for induction motor," in *Proc. IEEE Annu. Conf. Industrial Electronics Soc.*, vol. 3, 1998, pp. 1509–1514.

Guang Feng (S'00) received the B.Sc. degree in electrical engineering and the Ph.D. degree in power electronics from Tsinghua University, Beijing, China, in 1995 and 2000, respectively.

Since September 2000, he has been a Research Assistant in Queen's Power Group, Queen's University, Kingston, ON, Canada. His research interests include digital control of switching power converters, power factor correction techniques, and adjustable-speed motor drives.

Yan-Fei Liu (S'91–M'94–SM'97) received the B.Sc. and M.Sc. degrees from the Department of Electrical Engineering, Zhejiang University, Hangzhou, China, in 1984 and 1987, respectively, and the Ph.D. degree from the Department of Electrical and Computer Engineering, Queen's University, Kingston, ON, Canada, in 1994.

Since August 1999, he has been an Associate Professor with the Department of Electrical and Computer Engineering, Queen's University. From 1994 to 1999, he was a Technical Advisor with the Advanced Power System Division, Astec (formerly Nortel Networks), where he was responsible for high quality design, new products, and technology development. His research interests include digital control technologies for dc–dc switching converters and ac–dc converters with power factor correction, EMI filter design methodologies for switching converters, topologies and controls for high switching frequency, low switching loss converters, modeling and analysis of core loss and copper loss for high frequency planar magnetics, topologies and control for VRM, and large signal modeling of switching converters.

Dr. Liu received the Premiere's Research Excellent Award (PREA) in 2001, the Golden Apple Teaching Award in 2000, both in Queen's University, and the Award in Excellence in Technology from Nortel in 1997.

Lipei Huang was born in Jiangsu, China, on July 12,1946. He received the B.E. and M.E. degrees in electrical engineering from Tsinghua university, Beijing, China, in 1970 and 1982, respectively, and the Ph.D. degree from Meiji University, Tokyo, Japan, in 1996.

In 1970, he joined the Department of Electrical Engineering, Tsinghua University. From 1990 to 1994, he was an Associate Professor at Tsinghua University. Since 1994, he has been a Professor in the Department of Electrical Engineering, Tsinghua University. In 1987, he was a Visiting Scholar of Electrical Engineering at the Tokyo Institute of Technology, for three months, and at Meiji University, Kawasaki, Japan, for nine months. He joined the research projects of K.Matsuse Laboratory, Department of Electrical Engineering, Meiji University, Kawasaki, Japan, as a Visiting Professor in 1993. His research interests are in power electronics and adjustable-speed drives.

Dr. Huang received the Education Awards from the China Education Commission and Beijing People's Government in 1997. He is currently a Delta Scholar and a member of the China Electrotechnical Society.